

# Magnetosubbands of semiconductor quantum wires with Rashba and Dresselhaus spin-orbit coupling

Shengli Zhang, Run Liang, Erhu Zhang, Lei Zhang, and Yachao Liu

*Department of Applied Physics, Xi'an Jiaotong University, Xi'an 710049, People's Republic of China*

(Received 10 November 2005; published 17 April 2006)

The energy band structure of quantum wires with both Rashba and Dresselhaus spin-orbit couplings in a magnetic field is studied theoretically. We find that the magnetic field strongly affects the subband structure of the wire. With both couplings we obtain a beating pattern in the magnetoresistance. Compared with the quantum wire with only Rashba spin-orbit coupling, the beating pattern can be suppressed even if the coupling strengths are large. This is due to the interplay of the two spin-orbit couplings. The disappearing threshold of the nodes depends on both coupling strengths. When the coupling strengths change, the number of nodes of the beating pattern also varies.

DOI: [10.1103/PhysRevB.73.155316](https://doi.org/10.1103/PhysRevB.73.155316)

PACS number(s): 73.63.Nm, 72.25.Dc, 71.70.Ej, 85.75.-d

Spin-polarized electron transport phenomena have attracted considerable interest in recent years because of their potential application to information technology.<sup>1,2</sup> A lot of spintronic devices have been proposed with lower power consumption, higher speed, and a higher degree of functionality.<sup>3-6</sup> Most of these devices are proposed to manipulate electron spin via spin-orbit (SO) coupling. Among the device proposals a paradigmatic one is the spin-field-effect transistor (SFET) proposed by Datta and Das.<sup>3</sup> It utilizes the Rashba SO coupling to control the electron spin rotation while passing through the device. The strength of the Rashba SO coupling can be tuned by changing the gate voltage,<sup>7-10</sup> so that the final spin orientation of electrons can be controlled. This type of coupling arises from the structure inversion asymmetry of the confining potential of the two-dimensional electron gas (2DEG).<sup>11</sup>

In order to improve the efficiency of the SFET, electrons are confined in quasi-one-dimensional (quasi-1D) systems.<sup>12-14</sup> The effect of the interplay of the Rashba SO coupling and a magnetic field in quasi-1D systems has been studied both theoretically<sup>15-17</sup> and experimentally.<sup>18,19</sup> The research shows that the interaction of the Rashba SO coupling and the magnetic field can significantly modify the band structure. A beating pattern can exist in the magnetoresistance even in quasi-1D systems. Recently, Knobbe and Schäpers have calculated the subbands of semiconductor quantum wires with Rashba SO coupling in a perpendicular magnetic field.<sup>20</sup> They concluded that the shape of the beating patterns in the magnetoresistance strongly depends on the wire width.

Except for Rashba coupling, the Dresselhaus coupling also contributes to the SO interaction. This type of coupling stems from the bulk inversion asymmetry (BIA).<sup>21,22</sup> While the Rashba term usually dominates in narrow-gap materials,<sup>23</sup> the Dresselhaus term always dominates in wide-gap systems.<sup>24</sup> It has been demonstrated that the strengths of the Rashba and Dresselhaus couplings can be tuned to be equal, in which case the SFET can be stable to effects of spin-independent scattering.<sup>5</sup> Recently Tarasenko and Averkiev have investigated the interaction of the Rashba term and the BIA term in 2DEG and found that the interaction of the

two SO couplings can suppress the beats in the magnetoresistance.<sup>25</sup>

The effects of Dresselhaus SO coupling or both Rashba and Dresselhaus couplings are still challenging for the quasi-1D electron system. In order to determine how the interaction of Rashba and Dresselhaus terms affect the transport properties of the quantum wires in a magnetic field, we investigate the magnetosubbands of quantum wires with both SO couplings. Our calculation shows that the magnetic field strongly affects the energy subbands and the density of states at the Fermi energy level. With both SO couplings a beating pattern also appears in the magnetoresistance. However, unlike the wire with only the Rashba SO coupling, the beating pattern can be suppressed even though the total characteristic SO energy is large. This is due to the interplay of the two couplings. The change of Fermi energy also modifies the node position and the threshold of the coupling strength where the beating pattern appears or vanishes. That is totally different from the behaviors of quantum wires only with Rashba SO coupling.<sup>20</sup>

We consider a ballistic quantum wire, which is generated when a 2DEG is further confined in one direction. The confining potential is assumed to be parabolic. Here we choose the wire plane to be the  $xy$  plane with  $y$  direction parallel to the wire, so the form of the confining potential is  $V(x) = m^* \omega_0^2 x^2 / 2$ . The applied magnetic field is parallel to the  $z$  direction (Fig. 1), with corresponding magnetic vector potential  $\vec{A} = Bx\hat{e}_y$  in the Landau gauge. The Hamiltonian of the electron system reads

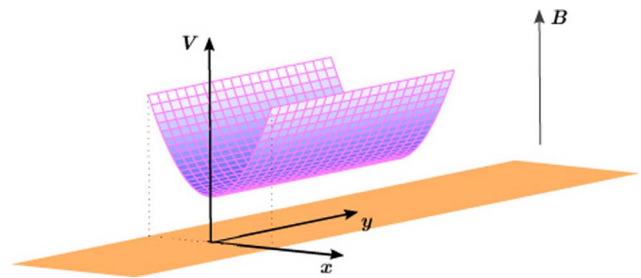


FIG. 1. (Color online) The model of the quantum wire structure.

$$H = H_0 + H_{so} = H_0 + H_R + H_D, \quad (1)$$

with

$$H_0 = \frac{1}{2m^*} [P_x^2 + (P_y - eBx)^2] + V(x) + \frac{1}{2} g \mu_B B \sigma_z, \quad (2)$$

$$H_R = \frac{\alpha}{\hbar} [\sigma_x (P_y - eBx) - \sigma_y P_x], \quad (3)$$

$$H_D = \frac{\beta}{\hbar} [\sigma_x P_x - \sigma_y (P_y - eBx)], \quad (4)$$

where  $m^*$  and  $g$  are the effective electron mass and Landé factor, respectively,  $\sigma_x$ ,  $\sigma_y$ , and  $\sigma_z$  are the Pauli matrices.  $H_R$  denotes the Rashba term and  $H_D$  corresponds to the Dresselhaus term,  $\alpha$  and  $\beta$  denote the Rashba and Dresselhaus coupling strength, respectively.

Since the electron is free in the  $y$  direction, we can assume the electron eigenfunction as follows:

$$\Psi(x, y) = \phi(x) \exp(ik_y y). \quad (5)$$

The Hamiltonian without SO couplings becomes<sup>20,26</sup>

$$H_0 = -\frac{\hbar^2}{2m^*} \frac{d^2}{dx^2} + \frac{1}{2} m^* \omega^2 (x - x_0)^2 + \frac{\omega_0^2 \hbar^2 k_y^2}{\omega^2 2m^*} + \frac{1}{2} g \mu_B B \sigma_z, \quad (6)$$

in which  $\omega = (\omega_0^2 + \omega_c^2)^{1/2}$  with the cyclotron frequency  $\omega_c = eB/m^*$ ,  $x_0 = (\omega_c/\omega)^2 (\hbar k_y / eB)$  is the center position of the harmonic oscillator, and  $m^*(\omega/\omega_0)^2$  can be referred to as an effective magnetic mass of the system.<sup>26</sup>

To solve the Schrödinger equation without SO coupling,  $H_0 \phi_{n\sigma}(x) = E_{n\sigma}^{(0)} \phi_{n\sigma}(x)$ , we obtained the set of eigenfunctions of  $H_0$ ,

$$\phi_{n\sigma}(x) = \frac{1}{\sqrt{b}} \frac{\pi^{-1/4}}{\sqrt{2^n n!}} H_n \left( \frac{x - x_0}{b} \right) \exp \left( -\frac{(x - x_0)^2}{2b^2} \right) \chi_\sigma, \quad (7)$$

$$n = 0, 1, 2, \dots; \quad \sigma = \pm,$$

where  $b = \sqrt{\hbar/m^* \omega}$  is the characteristic length of the harmonic oscillator.  $H_n(x)$  denotes the  $n$ th Hermite polynomial,  $\chi_+ = \begin{pmatrix} 1 \\ 0 \end{pmatrix}$  and  $\chi_- = \begin{pmatrix} 0 \\ 1 \end{pmatrix}$  are the eigenstates of  $\sigma_z$ . The corresponding eigenvalues of  $H_0$  are

$$E_{n\pm}^{(0)}(k_y) = \left[ \left( n + \frac{1}{2} \right) \hbar \omega + \frac{\hbar^2}{2m^*} \frac{\omega_0^2}{\omega^2} k_y^2 \pm \frac{1}{2} g \mu_B B \right]. \quad (8)$$

Now we consider the SO part of the Hamiltonian. With the ansatz eigenfunction given by Eq. (5),  $H_{so} = H_R + H_D$  becomes

$$H_R = \alpha \left[ \sigma_x \left( k_y - \frac{eB}{\hbar} x \right) + i \sigma_y \frac{d}{dx} \right], \quad (9)$$

$$H_D = \beta \left[ -i \sigma_x \frac{d}{dx} - \sigma_y \left( k_y - \frac{eB}{\hbar} x \right) \right]. \quad (10)$$

By expanding  $\phi(x) = \sum_{n,\sigma} a_{n,\sigma} \phi_{n,\sigma}(x)$  in terms of the eigenfunctions of  $H_0$ , the Schrödinger equation  $H\Psi = E\Psi$  becomes

$$(E_{n,\sigma}^{(0)} - E) a_{n,\sigma} + \sum_{m,\sigma' \neq \sigma} (H_{so})_{nm}^{\sigma\sigma'} a_{m\sigma'} = 0, \quad (11)$$

where the matrix elements  $(H_{so})_{nm}^{\sigma\sigma'} = \langle \phi_{n\sigma} | H_{so} | \phi_{m\sigma'} \rangle = \langle \phi_{n\sigma} | H_R | \phi_{m\sigma'} \rangle + \langle \phi_{n\sigma} | H_D | \phi_{m\sigma'} \rangle$  are given by

$$(H_R)_{nm}^{\pm\mp} = \alpha k_y \frac{\omega_0^2}{\omega^2}, \quad (12)$$

$$(H_R)_{nm}^{\pm\mp} = \frac{\alpha}{b} \left( -\frac{\omega_c}{\omega} \pm 1 \right) \sqrt{\frac{n+1}{2}} \delta_{n,m-1} + \frac{\alpha}{b} \left( -\frac{\omega_c}{\omega} \mp 1 \right) \sqrt{\frac{n}{2}} \delta_{n,m+1}, \quad n \neq m, \quad (13)$$

$$(H_D)_{nm}^{\pm\mp} = \pm i \beta k_y \frac{\omega_0^2}{\omega^2}, \quad (14)$$

$$(H_D)_{nm}^{\pm\mp} = -i \frac{\beta}{b} \left( \pm \frac{\omega_c}{\omega} + 1 \right) \sqrt{\frac{n+1}{2}} \delta_{n,m-1} - i \frac{\beta}{b} \left( \pm \frac{\omega_c}{\omega} - 1 \right) \sqrt{\frac{n}{2}} \delta_{n,m+1}, \quad n \neq m. \quad (15)$$

While  $(H_R)_{nm}^{\sigma\sigma'}$  and  $(H_D)_{nm}^{\sigma\sigma'}$  couple different spin states of the  $n$ th subband,  $(H_R)_{nm}^{\sigma\sigma'}$  and  $(H_D)_{nm}^{\sigma\sigma'}$  couple different spins of the neighboring subbands. By giving  $B$  and  $k_y$ , the full Hamiltonian eigenvalues can be calculated by solving the set of equations of Eq. (11).

When no magnetic field is applied and  $k_y=0$ , the subbands are still spin degenerate. However, the eigenenergies of the system are uniformly shifted downward by  $\Delta_{so} = \Delta_{so}^R + \Delta_{so}^D$ , which is the total characteristic SO energy,  $\Delta_{so}^R = m^* \alpha^2 / (2\hbar^2)$  (Ref. 13) and  $\Delta_{so}^D = m^* \beta^2 / (2\hbar^2)$  are the characteristic Rashba and Dresselhaus SO energy, respectively. This can be directly derived by setting  $k_y=0$  in the Hamiltonian (1).

In order to determine how the interaction of the two SO couplings affects the energy spectra, we calculated the energy levels of the quantum wires without magnetic field. Figure 2(a) shows the energy dispersion with relatively weak SO coupling. When  $\Delta_{so}^R / \hbar \omega_0 = 0.01$  and  $\Delta_{so}^D / \hbar \omega_0 = 0.005$ , the spin degeneracy at  $k \neq 0$  has been lifted. However, since the SO coupling is very weak, the coupling of different subbands does not occur obviously. For strong SO coupling, when  $\Delta_{so}^R / \hbar \omega_0 = 0.75$  and  $\Delta_{so}^D / \hbar \omega_0 = 0.25$ , the situation is completely different. As shown in Fig. 2(b), one can see a significant anticrossing. It arose from the strong coupling of neighboring subbands, which is described by the larger off-diagonal elements  $(H_{so})_{nm}^{\pm\mp}$ . In Fig. 2(c), where  $\Delta_{so}^R = \Delta_{so}^D = 0.5\hbar\omega_0$ , the anticrossing still exists. This is different from the results of Schliemann *et al.*<sup>5</sup> In fact, the spinor we choose is the eigenstate of  $\sigma_z$ , but Schliemann *et al.* choose the spinor as the eigenstate of  $H_{so}$ . This results in the difference of the spin character of the energy subbands in our research and Ref. 5. It also can be seen from Fig. 2 that the energy at the degeneracy points at  $k_y=0$  shifts downward by  $\Delta_{so} = \Delta_{so}^R + \Delta_{so}^D$ , compared to the system with no SO coupling.

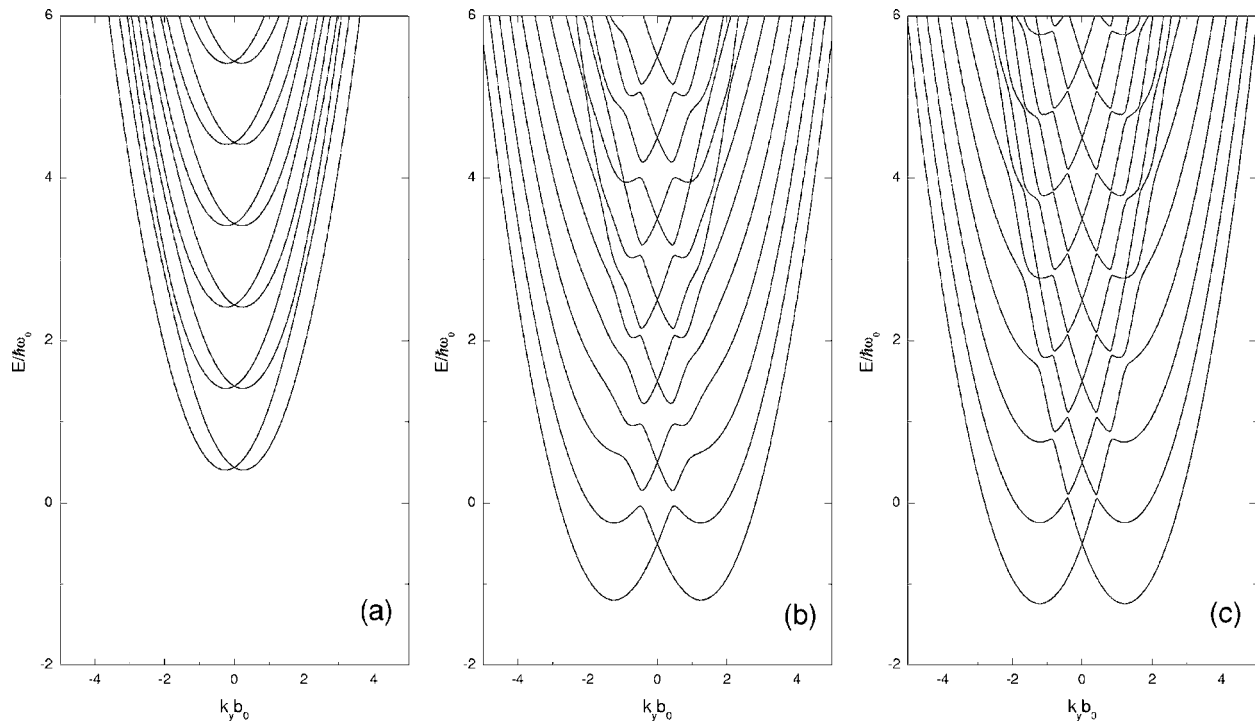


FIG. 2. Spectra of quantum wire at  $B=0$  with different Rashba and Dresselhaus SO coupling strength. (a)  $\Delta_{so}^R/\hbar\omega_0=0.01$  and  $\Delta_{so}^D/\hbar\omega_0=0.005$ . (b)  $\Delta_{so}^R/\hbar\omega_0=0.75$  and  $\Delta_{so}^D/\hbar\omega_0=0.25$ . (c)  $\Delta_{so}^R/\hbar\omega_0=0.5$  and  $\Delta_{so}^D/\hbar\omega_0=0.5$ . In (b) and (c), the anticrossing can be seen significantly.

We consider the energy spectrum of the wire in a magnetic field. Figure 3 shows how the magnetic field affects the energy subbands. Figure 3(a) shows the energy spectrum with  $\Delta_{so}^R/\hbar\omega_0=0.1$  and  $\Delta_{so}^D/\hbar\omega_0=0.05$ , while in Fig. 3(d),

$\Delta_{so}^R/\hbar\omega_0=\Delta_{so}^D/\hbar\omega_0=0.075$ . We can see that in both subbands anticrossing exists at zero magnetic fields. However, as the total characteristic SO energy here is smaller than that in Fig. 2(b), the anticrossing is correspondingly weaker. The energy

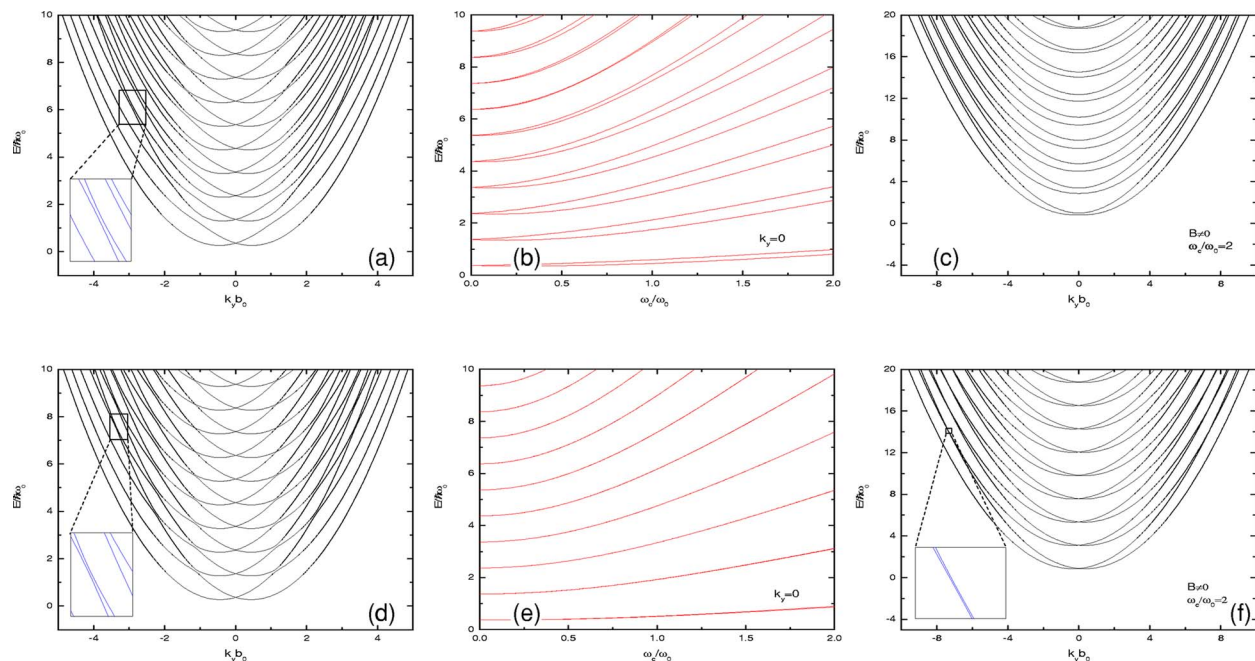


FIG. 3. (Color online) (a) Energy dispersion at zero magnetic field with  $\Delta_{so}^R/\hbar\omega_0=0.1$  and  $\Delta_{so}^D/\hbar\omega_0=0.005$ . The insets show the lower subbands anticrossing. (b) Energy spectrum of the same quantum wire as a function of  $\omega_c/\omega_0$ . The Zeeman energy splitting is chosen to be  $g\mu_B B = -0.015\hbar\omega_c$ . (c) Energy dispersion of the wire at a finite magnetic field (with  $\omega_c/\omega_0=2$ ). (d)–(e) The same energy spectrum as in (a)–(c), with a different SO coupling strength:  $\Delta_{so}^R/\hbar\omega_0=\Delta_{so}^D/\hbar\omega_0=0.075$ .

spectrum for  $k_y=0$  as a function of  $\omega_c/\omega_0$  is plotted in Figs. 3(b) and 3(e). Because  $\omega_c=eB/m^*$ , these figures show the relation between energy spectrum and applied magnetic field. When the magnetic field increases, the subband separation become larger owing to an increasing  $\hbar\omega$ . In both Figs. 3(b) and 3(e), the previous spin degeneracy at  $k_y=0$  is lifted when a magnetic field is applied to the wire. It is due to the broken time reversal symmetry. In Fig. 3(e) we can observe that the energy levels of the same state  $n$  with opposite spins do not separate significantly, which is different from Fig. 3(b). This is because the two coupling terms can cancel each other, giving a vanishing spin splitting in certain  $k$ -space directions.<sup>27</sup> Figures 3(c) and 3(f) show the energy dispersion at a finite magnetic field. In Fig. 3(c), the anticrossing no longer exists. It is different from the case at zero magnetic field. In Fig. 3(f), however, although much weaker, the anticrossing can still be seen. The interaction of SO coupling and the magnetic field leads to a rather complex energy spectrum, in which energy spacings between different subbands vary at a fixed magnetic field. It leads to a characteristic beating pattern in the magnetoresistance. Note the axes in Figs. 3(c) and 3(f) have different scales with the axes in Figs. 3(a) and 3(d). The slopes of the dispersions in Figs. 3(c) and 3(f) are smaller than that in Figs. 3(a) and 3(d). This is because the effective magnetic mass is larger when applied to a magnetic field.<sup>28,20</sup>

In order to confirm the characters of concrete materials, we apply the parameters of the material in the following. For the GaAs/AlGaAs 2DEG, the strengths of the Rashba and Dresselhaus SO coupling can be tuned to be equal.<sup>29,30</sup> In this paper, the Rashba and Dresselhaus coupling parameters are chosen to be vary from 0 to  $10 \times 10^{-12}$  eV m, which is in the same order of recent experiments.<sup>30</sup> The electron effective mass  $m^*=0.067m_e$ . We get the Fermi energy of the system  $E_{F,2D}=25$  meV by choosing a sample of the 2DEG concentration  $n_{2D}=7.0 \times 10^{15}$  m<sup>-2</sup>. We choose  $g=-0.44$  as the effective value. As discussed by Knobbe and Schäpers in Ref. 20, we assume that the Fermi energy of the quantum wire  $E_{F,1D}=E_{F,2D}$ , and does not vary as the magnetic field changes, for the sake of simplicity.

It is well known that the oscillations in the magnetoresistance of a quantum wire are directly related to the density of states at the Fermi energy level.<sup>26</sup> We calculated the density of states at the Fermi energy level as a function of the magnetic field. Figure 4(a) shows the density of states of a quantum wire with  $\hbar\omega_0=0.5$  meV, in which the Rashba and Dresselhaus coupling parameters are chosen to be  $10 \times 10^{-12}$  eV m and  $5 \times 10^{-12}$  eV m, respectively. The magnetoelectric subbands depopulated successively as the magnetic field increases. When the Fermi energy passes through the bottom of the subbands, a peak occurs in the density of states. By assuming the subband broadening  $\Gamma=0.2$  meV, we obtained a beating pattern in the DOS as Fig. 4(b), with each peak of the DOS corresponding to a pair of spin levels. Four nodes occur in the beating pattern when magnetic fields are 0.18 T, 0.30 T, 0.54 T, and 0.67 T, respectively. This beating pattern in the DOS qualitatively shows the conductivity oscillations.

By using the same steps we now consider how the strengths of Rashba and Dresselhaus terms affect the beating

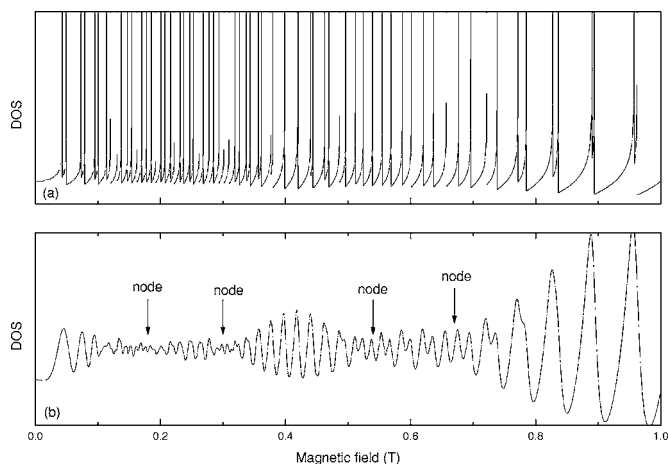


FIG. 4. (a) Density of states of a quantum wire as a function of the magnetic field with  $\hbar\omega_0=0.5$  meV and a fixed Fermi energy of 25 meV. The Rashba and Dresselhaus coupling strength is chosen to be  $10 \times 10^{-12}$  eV m and  $5 \times 10^{-12}$  eV m, respectively. (b) Density of states for subband broadening  $\Gamma=0.2$  meV. Four nodes occur at about 0.18 T, 0.30 T, 0.54 T, and 0.67 T, respectively.

pattern of the magnetoresistance. First we calculated the energy spectrum at  $k_y=0$  as a function of the magnetic field for different Rashba strengths or Dresselhaus strengths. Figures 5(a)–5(c) show the energy spectrum of a wire with  $\hbar\omega_0=0.5$  meV, Dresselhaus SO coupling strength  $\beta=3 \times 10^{-12}$  eV m, and Rashba SO coupling strength  $\alpha=1 \times 10^{-12}$  eV m,  $4 \times 10^{-12}$  eV m,  $10 \times 10^{-12}$  eV m, respectively. As mentioned above, the magnetoresistance is directly related to the density of states at the Fermi energy level.<sup>26</sup> Each time the bottom of a subband at  $k_y \approx 0$  crosses the Fermi energy level, a maximum of conductance is observed. A node is observed in the magnetoresistance if the subbands crossing the Fermi energy level are spaced equally. In the nanowire with  $\hbar\omega_0=0.5$  meV and  $\beta=3 \times 10^{-12}$  eV m, we can observe two nodes when  $\alpha=1 \times 10^{-12}$  eV m, when magnetic fields are 0.22 T and 0.43 T, and four nodes when  $\alpha=10 \times 10^{-12}$  eV m, at 0.08 T, 0.26 T, 0.45 T, and 0.66 T, respectively. Figure 5(b) shows the energy spectrum of a wire with sublevel spacing  $\hbar\omega_0=0.5$  meV, Dresselhaus SO coupling strength  $\beta=3 \times 10^{-12}$  eV m, and Rashba SO coupling strength  $\alpha=4 \times 10^{-12}$  eV m. The spin splitting is very small. No nodes exist in the magnetoresistance.

In Fig. 5(d), we can see that the nodes gradually merge and then appear again as  $\alpha$  grows from 0 to  $10 \times 10^{-12}$  eV m. For larger  $\alpha$ , more nodes exist in the magnetoresistance. This is due to the interaction of Rashba and Dresselhaus SO coupling. First, as the Rashba SO coupling strength  $\alpha$  increases, it offsets the Dresselhaus term. The interaction gives a gradually smaller spin splitting of the sublevels. At certain  $\alpha$ , the nodes finally disappeared. When  $\alpha$  grows larger than  $\beta$ , the spin splitting of the subbands grows gradually, and the nodes appear again when  $\alpha$  grows large enough. At even larger  $\alpha$ , more nodes exist. This is because the contribution of geometrical confinement to the level spacing is comparatively small as  $\alpha$  gets larger.

As the nodes positions of magnetoresistance of quantum wires depends on the interaction of the Rashba and Dressel-

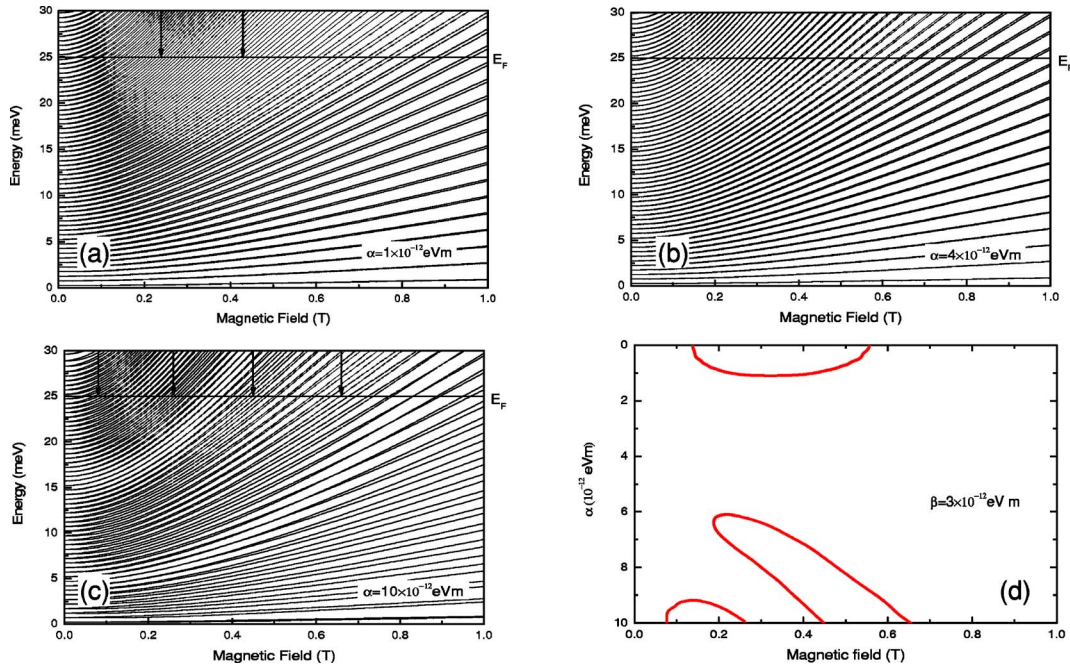


FIG. 5. (Color online) (a)–(c) Energy spectra at  $k_y=0$  as a function of the magnetic field, with  $\hbar\omega_0=0.5$  meV,  $\beta=3 \times 10^{-12}$  eV m and  $\alpha=1 \times 10^{-12}$  eV m,  $4 \times 10^{-12}$  eV m and  $10 \times 10^{-12}$  eV m, respectively. Arrows denote the magnetic field where the nodes occur. (d) The node's positions in the magnetoresistance, as a function of the Rashba SO coupling strength.

haus SO coupling, we calculated the node's positions for different  $\beta$  as  $\alpha$  increases, in which the range of magnetic field we considered here is from 0 to 1 T. Figures 6(a)–6(c) show the nodes positions as  $\alpha$  increases with  $\beta=3$

$\times 10^{-12}$  eV m,  $5 \times 10^{-12}$  eV m, and  $7.5 \times 10^{-12}$  eV m, respectively. In Figs. 6(a) and 6(b), as  $\alpha$  grows from 0, the separation of the nodes gets smaller, and merge at  $\alpha=1.1 \times 10^{-12}$  eV m in Fig. 6(a) and  $\alpha=2.1 \times 10^{-12}$  eV m in Fig.

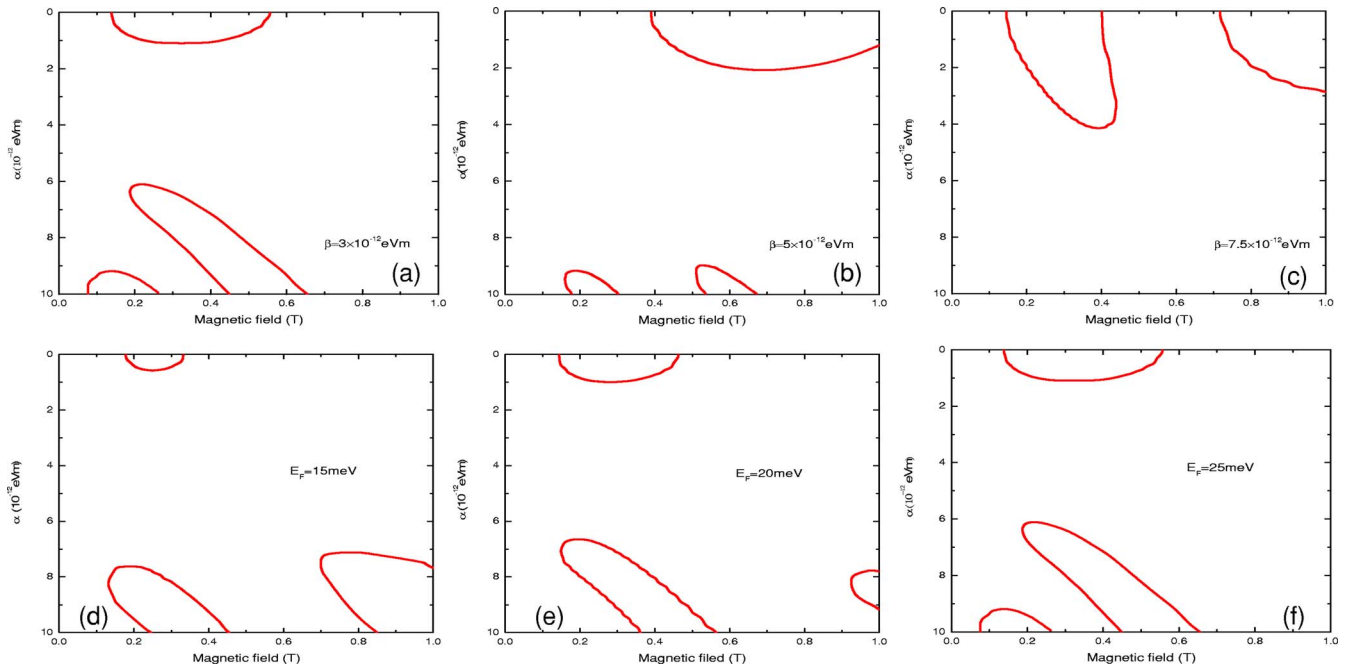


FIG. 6. (Color online) (a)–(c) Node positions in the magnetoresistance as a function of Rashba SO coupling strength with  $E_{F,1D}=25$  meV and  $\beta=3 \times 10^{-12}$  eV m,  $5 \times 10^{-12}$  eV m, and  $7.5 \times 10^{-12}$  eV m, respectively. The disappearing threshold of  $\alpha$  of the nodes is  $1.1 \times 10^{-12}$  eV m to  $6.1 \times 10^{-12}$  eV m in (a) and  $2.1 \times 10^{-12}$  eV m to  $8.9 \times 10^{-12}$  eV m in (b). The nodes disappear at  $\alpha=4.2 \times 10^{-12}$  eV m and do not exist again in (c). (d)–(f) Nodes positions in the magnetoresistance for  $E_{F,1D}=15$  meV, 20 meV, and 25 meV, respectively. The Dresselhaus SO coupling strength is chosen to be  $\beta=3 \times 10^{-12}$  eV m. The disappearing threshold of  $\alpha$  of the nodes is  $0.6 \times 10^{-12}$  eV m to  $7.1 \times 10^{-12}$  eV m in (d),  $1.0 \times 10^{-12}$  eV m to  $6.5 \times 10^{-12}$  eV m in (e) and  $1.1 \times 10^{-12}$  eV m to  $6.1 \times 10^{-12}$  eV m in (f).

6(b). When  $\alpha$  grows larger, the nodes first disappear and then exist again at  $\alpha=6.1 \times 10^{-12}$  eV m in Fig. 6(a) and  $\alpha=8.9 \times 10^{-12}$  eV m in Fig. 6(b). Then the nodes shift towards larger magnetic fields and the separation also grows larger as  $\alpha$  increases. More nodes occur when  $\alpha$  grows even larger. This happens coincidentally at  $\alpha=9.1 \times 10^{-12}$  eV m in both Figs. 6(a) and 6(b). In Fig. 6(c), when  $\alpha=0$  eV m, there are three nodes existing in the magnetoresistance. As  $\alpha$  increase, the first two nodes get close to each other and all the three nodes shift toward larger magnetic field. The nodes merge at  $\alpha=4.2 \times 10^{-12}$  eV m and do not exist again as  $\alpha$  increases in the range considered here. Thus, in Figs. 6(a)–6(c), as  $\beta$  increases, the thresholds of  $\alpha$  where the nodes disappear also move towards larger values.

Figures 6(d)–6(f) show the node's positions as  $\alpha$  increases with different Fermi energy  $E_F$ , and the Dresselhaus coupling strength  $\beta$  is chosen to be  $3 \times 10^{-12}$  eV m. The thresholds of  $\alpha$  where the nodes disappear are  $0.6 \times 10^{-12}$  eV m,  $1.0 \times 10^{-12}$  eV m, and  $1.1 \times 10^{-12}$  eV m in Figs. 6(d)–6(f), respectively. When  $\alpha$  is smaller than the threshold, the separation of the nodes enlarges as  $E_F$  increases. The threshold of  $\alpha$  where the nodes exist again is  $7.1 \times 10^{-12}$  eV m,  $6.6 \times 10^{-12}$  eV m, and  $6.1 \times 10^{-12}$  eV m in Figs. 6(d)–6(f), respectively. That is, as  $E_F$  increases, the threshold of  $\alpha$  where the nodes disappear grows larger, while the threshold of  $\alpha$  where the nodes exist again gets smaller. This is totally different from the result of wire with only Rashba SO coupling.<sup>20</sup>

We also calculated the node positions as  $\beta$  increases for different  $\alpha$  and different Fermi energy. The corresponding figures are almost the same as Fig. 6.

For comparison, we also calculated the density of states of a very wide wire,  $\hbar\omega_0=0.01$  meV, and a very narrow wire,  $\hbar\omega_0=23$  meV, as a function of the magnetic field. Figure 7(a) shows the density of states of the wide wire, and the Rashba and Dresselhaus coupling parameters are chosen to be  $10 \times 10^{-12}$  eV m and  $5 \times 10^{-12}$  eV m, respectively. In such a wide wire, several nodes exist in the beating pattern. When the magnetic field strength grows from 0.2 T to 1 T, ten nodes exist in the beating pattern, the corresponding magnetic field strengths are 0.21 T, 0.23 T, 0.25 T, 0.28 T, 0.31 T, 0.35 T, 0.42 T, 0.49 T, 0.64 T, and 0.77 T. When the two SO coupling strengths are chosen to be equal, no nodes exist at all [see in Fig. 7(b), where  $\alpha=\beta=3 \times 10^{-12}$  eV m]. This is consistent with recent research on 2D electron gas.<sup>31</sup> Here, we conclude, the appearance and disappearance of nodes in the magnetoresistance is the same in the 2D electron gas as in the quantum wires. In a very narrow wire, as the subbands' separations are so large, only a few or even no subband will pass the Fermi energy level as the magnetic field increases, so the magnetoresistance will not oscillate drastically. In the 1D limit, only the  $n=0$  subband is below the Fermi energy level, no oscillates exist at all. Figures 7(c) and 7(d) show the density of states of a very narrow wire,  $\hbar\omega_0=23$  meV, where in Fig. 7(c),  $\alpha=10 \times 10^{-12}$  eV m,  $\beta=5 \times 10^{-12}$  eV m, and in Fig. 7(d),  $\alpha=\beta=3 \times 10^{-12}$  eV m, we can see that no oscillates exist and the magnetoresistance looks the same in the two situations. This is because the subbands separate so much that the coupling of different subbands caused by the SO coupling terms can be ignored.

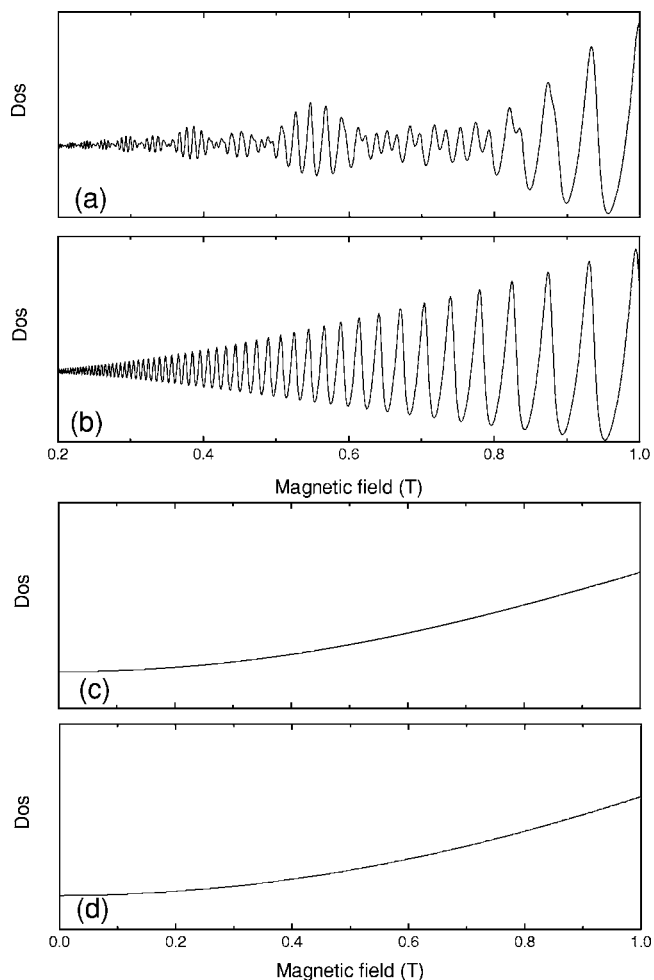


FIG. 7. (a) and (b) Density of states of a wide quantum wire,  $\hbar\omega_0=0.01$  meV, as a function of the magnetic field. Note in (a) and (b) the magnetic field varies from 0.2 T to 1 T. (a) The Rashba and Dresselhaus SO coupling strength is chosen to be  $\alpha=10 \times 10^{-12}$  eV m and  $\beta=5 \times 10^{-12}$  eV m, respectively. Ten nodes exist in the beating pattern in the magnetic field considered here, the corresponding magnetic field strengths are 0.21 T, 0.23 T, 0.25 T, 0.28 T, 0.31 T, 0.35 T, 0.42 T, 0.49 T, 0.64 T, and 0.77 T. (b)  $\alpha=\beta=3 \times 10^{-12}$  eV m. No nodes exist in the DOS. (c) and (d) Density of states of a narrow quantum wire,  $\hbar\omega_0=23$  meV, as a function of the magnetic field. (c) Rashba SO coupling strength  $\alpha=10 \times 10^{-12}$  eV m, Dresselhaus SO coupling strength  $\beta=5 \times 10^{-12}$  eV m. (d)  $\alpha=\beta=3 \times 10^{-12}$  eV m.

It is significant to observe the emergence and disappearance of nodes of the beating pattern in the magnetoresistance as the theoretical results of this paper. One may use quantum wires with both Rashba and Dresselhaus SO couplings, such as GaAs/AlGaAs. The strengths of both Rashba and Dresselhaus SO couplings are controlled as Refs. 27 and 29. The behavior of the beating pattern in the magnetoresistance of quantum wires, especially the position shift and emergence or disappearance of the nodes, can be measured directly. We should point out that this behavior of the beating pattern does not depend on special materials. For other materials, if the two SO coupling strengths can be tuned from differ significantly to equal, this behavior can be observed.

In conclusion, we have investigated the effect of a perpendicular magnetic field on a quantum wire with both Rashba and Dresselhaus SO coupling. Without magnetic field the spin degeneracy is still preserved at  $k=0$ . When a nonzero magnetic field is applied, it breaks the time-reversal symmetry and lifts the corresponding degeneracy. We find that the energy spectrum strongly depends on the magnetic field and the strengths of both Rashba and Dresselhaus SO couplings. As the magnetic field increases, it gives a higher oscillation frequency, so it enlarges the separation of the subbands and thus weakens the SO coupling. The density of states at the Fermi energy level oscillates as the magnetic field increases, which causes a beating pattern in the magnetoresistance. At certain Dresselhaus SO coupling strength, as the Rashba SO

coupling constant  $\alpha$  increases from 0, the beating pattern first exists when  $\alpha$  is small, then vanishes when the strengths of the two SO couplings get close to each other, and then exists again when  $\alpha$  is much larger than the Dresselhaus SO coupling constant  $\beta$ . Thus, unlike the wire with only Rashba SO coupling, the beats in the magnetoresistance may disappear even when the total characteristic SO energy is large, due to the interaction of the two couplings. When one of the coupling strengths is large, there may be more nodes existing in the magnetoresistance.

We thank S. M. Zhao, J. Li, Z. W. Yao, Q. L. Xiang, and Q. Wang for helpful discussions. This work was supported by the NSF of China No. 10374075.

- 
- <sup>1</sup>S. A. Wolf, D. D. Awschalom, R. A. Buhrman, J. M. Daughton, S. von Molnár, M. L. Roukes, A. Y. Chtchelkanova, and D. M. Treger, *Science* **294**, 1488 (2001).
- <sup>2</sup>I. Žutić, J. Fabian, and S. D. Sarma, *Rev. Mod. Phys.* **76**, 323 (2004).
- <sup>3</sup>S. Datta and B. Das, *Appl. Phys. Lett.* **56**, 665 (1990).
- <sup>4</sup>X. F. Wang, P. Vasilopoulos, and F. M. Peeters, *Phys. Rev. B* **65**, 165217 (2002).
- <sup>5</sup>J. Schliemann, J. C. Egues, and D. Loss, *Phys. Rev. Lett.* **90**, 146801 (2003).
- <sup>6</sup>P. Štředa and P. Šeba, *Phys. Rev. Lett.* **90**, 256601 (2003).
- <sup>7</sup>B. Das, D. C. Miller, S. Datta, R. Reifenberger, W. P. Hong, P. K. Bhattacharya, J. Singh, and M. Jaffe, *Phys. Rev. B* **39**, 1411 (1989).
- <sup>8</sup>J. Nitta, T. Akazaki, H. Takayanagi, and T. Enoki, *Phys. Rev. Lett.* **78**, 1335 (1997).
- <sup>9</sup>G. Engels, J. Lange, Th. Schäpers, and H. Lüth, *Phys. Rev. B* **55**, R1958 (1997).
- <sup>10</sup>D. Grundler, *Phys. Rev. Lett.* **84**, 6074 (2000).
- <sup>11</sup>Yu. A. Bychkov and E. I. Rashba, *JETP Lett.* **39**, 78 (1984).
- <sup>12</sup>F. Mireles and G. Kirczenow, *Phys. Rev. B* **64**, 024426 (2001).
- <sup>13</sup>M. Governale and U. Zülicke, *Phys. Rev. B* **66**, 073311 (2002).
- <sup>14</sup>M. Governale, D. Boese, U. Zülicke, and C. Schroll, *Phys. Rev. B* **65**, 140403(R) (2002).
- <sup>15</sup>Y. Yu, Y. Wen, J. Li, Z. Su, and S. T. Chui, *Phys. Rev. B* **69**, 153307 (2004).
- <sup>16</sup>Y. V. Pershin, J. A. Nesteroff, and V. Privman, *Phys. Rev. B* **69**, 121306(R) (2004).
- <sup>17</sup>L. Serra, D. Sánchez, and R. López, *Phys. Rev. B* **72**, 235309 (2005).
- <sup>18</sup>Y. Sato, S. Gozu, T. Kikutani, and S. Yamada, *Physica B* **272**, 114 (1999).
- <sup>19</sup>Th. Schäpers, J. Knobbe, and V. A. Guzenko, *Phys. Rev. B* **69**, 235323 (2004).
- <sup>20</sup>J. Knobbe and Th. Schäpers, *Phys. Rev. B* **71**, 035311 (2005).
- <sup>21</sup>G. Dresselhaus, *Phys. Rev.* **100**, 580 (1955).
- <sup>22</sup>M. I. Dyakonov and V. I. Perel, *Sov. Phys. JETP* **33**, 1053 (1971).
- <sup>23</sup>J. Luo, H. Munekata, F. F. Fang, and P. J. Stiles, *Phys. Rev. B* **41**, 7685 (1990).
- <sup>24</sup>G. Lommer, F. Malcher, and U. Rossler, *Phys. Rev. Lett.* **60**, 728 (1988).
- <sup>25</sup>S. A. Tarasenko and N. S. Averkiev, *JETP Lett.* **75**, 552 (2002).
- <sup>26</sup>K.-F. Berggren, G. Roos, and H. van Houten, *Phys. Rev. B* **37**, 10118 (1988).
- <sup>27</sup>S. D. Ganichev, V. V. Bel'kov, L. E. Golub, E. L. Ivchenko, Petra Schneider, S. Giglberger, J. Eroms, J. De Boeck, G. Borghs, W. Wegscheider, D. Weiss, and W. Prettl, *Phys. Rev. Lett.* **92**, 256601 (2004).
- <sup>28</sup>K.-F. Berggren, T. J. Thornton, D. J. Newson, and M. Pepper, *Phys. Rev. Lett.* **57**, 1769 (1986).
- <sup>29</sup>J. B. Miller, D. M. Zumbühl, C. M. Marcus, Y. B. Lyanda-Geller, D. Goldhaber-Gordon, K. Campman, and A. C. Gossard, *Phys. Rev. Lett.* **90**, 076807 (2003).
- <sup>30</sup>E. Shafir, M. Shen, and S. Saikin, *Phys. Rev. B* **70**, 241302(R) (2004).
- <sup>31</sup>N. S. Averkiev, M. M. Glazov, and S. A. Tarasenko, *Solid State Commun.* **133**, 543 (2005).